Many-body approaches to the homogeneous electron gas in two dimensions

Gustav Baardsen,[1] Karl Leikanger,[2] Titus Morris,[3] Sarah Reimann,[2] Scott K. Bogner,[3] and Morten Hjorth-Jensen[1,3]

[1] *Department of Physics, University of Oslo, N-0316 Oslo, Norway*
[2] *Department of Chemistry and Center of Theoretical and Computational Chemistry, University of Oslo, N-0316 Oslo, Norway*
[3] *National Superconducting Cyclotron Laboratory and Department of Physics and Astronomy, Michigan State University, East Lansing, MI 48824, USA*

We present results for the two- and three-dimensional homogeneous electron gas using first principle methods like coupled cluster theory and two recently developed methods, the in-medium Similarity Renormalization Group approach and the full configuration interaction quantum Monte Carlo method of Booth and co-workers [1–3]. In particular, we present new results for the correlation energy for the two-dimensional electron gas and analyze our results in terms of finite size effects and basis functions.

PACS numbers: 02.70.Ss, 31.15.A-, 31.15.bw, 31.15.V-, 71.10.Ca, 71.15.-m

I. INTRODUCTION

A proper understanding of the role of correlations beyond a mean-field description is of great importance for quantum many-particle theories. For all possible quantum-mechanical systems, either finite ones or infinite systems like the homogeneous electron gas in two or three dimensions or nuclear or neutron star matter, the concept of an independent particle motion continues to play a fundamental role in studies of many-particle systems. Deviations from such an independent particle, or mean-field, picture have normally been interpreted as a possible measure of correlations. The latter are expected to reveal important features of both the structure and the dynamics of a many-particle system beyond a mean-field approximation.

The homogeneous electron gas is one of the few examples of a system of many interacting particles that allows for a solution of the mean-field Hartree-Fock equations on a closed form. To first order in the electron-electron interaction, this applies to ground state properties like the energy and its pertinent equation of state as well. The homogeneus electron gas is a system of electrons that is not influenced by external forces except by an attraction provided by a uniform background of ions. These ions give rise to a uniform background charge. The ions are stationary and the system as a whole is neutral. Irrespective of this simplicity, this system, in both two and three-dimensions, has eluded a proper description of correlations in terms of various first principle methods, except perhaps for quantum Monte Carlo methods. In particular, the diffusion Monte Carlo calculations of Ceperley *et al.* [4, 5], are presently still considered as the best possible benchmarks for the two- and three-dimensional electron gas.

The electron gas, in two or three dimensions is thus interesting as a test-bed for electron-electron correlations. The three-dimensional electron gas is particularly important as a cornerstone of the local-density approximation in density-functional theory. In the physical world, systems similar to the three-dimensional electron gas can be found in, for example, alkali metals and doped semiconductors. Two-dimensional electron fluids are observed on metal and liquid-helium surfaces, as well as at metal-oxide-semiconductor interfaces. However, the Coulomb interaction has an infinite range, and therefore long-range correlations play an essential role in the electron gas. At low densities, the electrons become localized and form a lattice. This so-called Wigner crystallization [6] is a direct consequence of the long-ranged repulsive interaction. At higher densities, the electron gas is better described as a liquid [4, 5, 7, 8]. When using, for example, Monte Carlo methods [9], the electron gas must be approximated by a finite system. The long-range Coulomb interaction in the electron gas causes additional finite-size effects [10–12] that are not present in other infinite systems like nuclear matter or neutron star matter in [13]. This poses additional challenges to many-body methods when applied to the electron gas.

The aim of this work is to present results for the infinite electron gas using several many-body methods. We focus in particular on coupled-cluster theory (add ref), the recently develop in-medium similarity renormalization group methods, full-configuration interaction quantmum Monte Carlo [1–3] We present results for all these methods and study in particular both finite size effects and effects due to a truncation in the single-particle basis (add more refs).

More

II. FORMALISM

A. Previous studies of the electron gas

The electron gas has been studied using a large number of different approaches, and we will here only mention some of the most important works that are relevant here. We start with the three-dimensional electron gas, which has got most attention in the literature. The three-dimensional electron gas will mainly serve as a benchmark for our calculations,

It is a well-kown fact that the correlation energy of the three-dimensional electron gas diverges at second order

in perturbation theory. The particle-hole ring diagrams dominate at the limit of high density. Even though all these diagrams diverge when calculated separately, the energy converges when summing all direct particle-hole ring diagrams to infinite order. Gell-Mann and Brueckner obtained for this so-called random-phase approximation (RPA) the first terms of the exact energy in the high-density limit [14].

At metallic and lower densities, short-ranged correlations become significant. Singwi *et al.* [15] and Lowy and Brown [16] came up with early attempts to combine RPA with contributions for short-ranged correlations. The calculations of Singwi *et al.* were based on dielectric function theory, whereas Lowy and Brown interpolated between short- and long-range models using a diagrammatic technique.

In 1978, Ceperley used [7] the variational Monte Carlo (VMC) method to study the two- and three-dimensional electron gas. The obtained VMC ground-state energies were shown to be close to other results at that time. Higher accuracy can be obtained with the diffusion Monte Carlo (DMC) method (in nuclear physics, this method is commonly named Green's function Monte Carlo). The DMC results of Ceperley and Alder from 1980 [4] are still, more than thirty years later, among the most accurate energy estimates for the three-dimensional electron gas. In Ref. [4], the fermion sign problem is handled using a released-node approximation. Similar accuracy has been obtained in more recent calculations using the backflow-correlation technique [17], which is used to relax the simpler fixed-node approximation.

When modelling the electron gas using a finite box, as is commonly done in Monte Carlo methods, the energy has an error compared to the electron gas at the thermodynamic limit. At the thermodynamic limit, plane-wave single-particle states fill the Fermi sphere with a continuous spectrum. When the system is approximated using a finite box, the single-particle spectrum becomes discrete. This discretization gives an error that is common to systems with short-ranged and long-ranged interactions. The perhaps most obvious way to correct for finite-size effects related to a discrete single-particle basis, is by using an extrapolation formula. As is described in Ref. [12], results from Hartree-Fock and density-functional theory calculations can be used to construct extrapolation methods. Another approach that efficiently reduces the finite-size error is a technique that utilizes so-called twisted boundary conditions [18]. Twisted boundary conditions means that the single-particle wave function is multiplied by a complex phase factor when moving from one simulation cell to a neighbouring cell. When averaging over results obtained with different twist angles, the energy estimates become much more accurate than when using periodic boundary conditions [18].

Finite-size approximations of extended Coulombic systems, such as the electron gas, have additional errors that are caused by the long-ranged interaction [10–12]. Interactions with electrons in neighbouring cells can be summed using, for example, Ewald's method [10, 12, 19, 20]. In Ewald's approach, each electron in the simulation cell interacts with an infinite number of image charges located at the same local position in all other cells. As is shown in Refs. [10, 11], Ewald's interaction cannot describe the exchange-correlation energy correctly. Chiesa *et al.* [11] used a static structure factor and a Jastrow factor derived from RPA to estimate the correction to Ewald's method. The correction technique of Chiesa *et al.* is directly applicable only to Monte Carlo methods. Fraser *et al.* [10] suggested two different effective interactions that avoid the screening effects caused by Ewald's interaction . The most successful alternative was to use a normal Coulomb interaction combined with the minimum-image convention [10]. The reader is referred to Ref. [12] for more details about finite-size effects and different approaches to correct for the related errors.

The full configuration-interaction quantum Monte Carlo (FCIQMC) method [1] is a new approach to the quantum many-body problem, in which the full configuration-interaction (FCI) equations [21] are solved approximately using a Monte Carlo technique. Similarly as in the DMC or GFMC methods, the Schrödinger equation is written as a diffusion equation with an imaginary time variable [2]. In the FCI method, the total wave-function ansatz is expressed as a linear combination of Slater determinants constructed from a given single-particle basis. In FCIQMC, the coefficients in the expansion of Slater determinants are obtained as the large-time limit of a random walk [2]. As we discussed above, Monte Carlo calculations of the electron gas have an error related to the finite number of particles in the simulation cell. Methods such as FCIQMC, CC, and partial summations derived from many-body perturbation theory have and additional error when studying systems with a discrete single-particle basis: The result depends on the given set of both occupied and unoccupied single-particle states [22]. This error can be corrected for by using, for example, the single-point extrapolation technique [22, 23] introduced by Shepherd *et al.* The FCIQMC method has recently been applied to finite electron-gas systems [2, 22, 23], giving results in close agreement with DMC calculations utilizing backflow correlations [2].

Singal and Das [24] were the first to study the electron gas using a CC approach. The approximation they used is similar to the BHF method [25], and does not properly include particle-hole ring diagrams. Later, Freeman did CC calculations [26] in which only ring diagrams and their exchange parts were retained in a CC doubles approximation. The results of both Singal and Das [24] and Freeman [26] compared well with dielectric-function approaches. Presently, the most accurate CC caclulations of the three-dimensional electron gas are those of Bishop and Lührmann [8, 27]. Bishop and Lührmann derived a CC SUB2 approximation (also called CC doubles (CCD) [28]) for the electron gas, extended with some ladder contributions from higher-order

amplitudes. As the authors describe in Ref. [27], the CCD approximation contains many more diagrammatic classes than partial-summation techniques derived from perturbation theory. The CCD approximation takes account of particle-particle and hole-hole ladders, particle-hole ring diagrams including exchange terms, and many other diagrams to infinite order in perturbation theory. In their CC approximations, Bishop and Lührmann replaced summations over hole states by averages. In fact, the nine-dimensional CC amplitudes were simplified to one-dimensional objects, with the absolute value of the transfer momentum being the only variable. The authors showed that the state-average approximation is accurate in the RPA approximation. Bishop and Lührmann neglected some diagrammatic classes, such as the hole-hole ladders and mixed ladders, which they assumed to be small. Despite all these approximations, the final CC energies are very accurate in a typical metallic density range. Relative differences of less than one percent compared to DMC calculations of Ceperley and Alder may indicate that the extended CCD approximation describes most of the relevant correlations in the three-dimensional electron gas [8].

The CC study of Bishop and Lührmann was very successful, but still the calculations are based on a large number of approximations. It would be desireable to apply CC theory to the electron gas without the same approximations. Recently, Shepherd *et al.* [22, 29–31] have taken up again the CC effort for the three-dimensional electron gas. The CC calculations for the electron gas from the 1970s and 1980s were all done at the thermodynamic limit [8, 24, 26, 27]. Unfortunately, singularities related to the Coulomb two-body interaction may complicate numerical calculations at the thermodynamic limit. Shepherd *et al.* approximate the electron gas using finite cubic boxes [22, 29–31]. When using finite-size systems, the CC equations are simpler and most of the problems with ill-bahaved functions are avoided. Instead, one has to deal with errors related to finite particle numbers and single-particle bases, similarly as in the FCIQMC method [2, 22, 23].

Let us finally turn our attention to the two-dimensional electron gas. The two-dimensional electron gas is defined in the same way as the three-dimensional counterpart, and similar approaches can therefore often be used to study both systems. As a first example, the classical derivation of the high-density RPA approximation by Gell-Mann and Brueckner [14] has been extended to the two-dimensional electron gas by Rajagopal and Kimball [32].

As far as we know, the only CC calculations that have been done for the two-dimensional electron gas are the ring [33] and particle-particle ladder [34] approximations of Freeman. Beacuse of stronger correlations in the purely two-dimensional system, the ring approximation was not as reliable in two dimensions as it was in the three-dimensional case [33]. According to the studies of Freeman, the CC ring-diagram approximation is less accurate than the CC ladder approximation at intermediate and low densities, whereas both methods give similar results at the high-density limit [34].

In the earliest CC studies of the electron gas [8, 24, 26, 27, 33, 34], the system was treated at the thermodynamic limit. Some of the most accurate calculations of the electron gas [2, 4, 5] have been done using finite boxes and Monte Carlo methods. Recently, CC theory has been applied in several studies [22, 29–31, 35] to finite-particle approximations of the homogeneous electron gas. Freeman has done CC studies of the two-dimensional electron gas including only ring [33] or only particle-particle ladder [34] diagrams from the CCD approximation, but to the best of our knowledge, nobody has done a complete CCD calculation of the two-dimensional homogeneous electron gas. As an extension of the CC calculations by Shepherd *et al.* [22, 29–31] and Roggero *et al.* [35], we study the two-dimensional electron gas in the CCD approximation using a finite number of particles. We validate our methods by comparing results for the three-dimensional electron gas with Shepherd *et al.* [22, 23]. using momentum discretized in cartesian coordinates, see discussions below.

B. Model Hamiltonian and Definitions

The homogeneous electron gas is defined as an infinite system consisting of electrons distributed with a constant density through the entire real space. The system is assumed to contain a constant positive background charge which cancels the negative charges of the electrons. The Hamiltonian operator of the homogeneous electron gas can be written as [36]

$$\hat{H} = \hat{H}_{\text{kin}} + \hat{H}_{ee} + \hat{H}_{eb} + \hat{H}_{bb}, \tag{1}$$

where $\hat{H}_{\text{kin}}$ is the kinetic-energy operator, $\hat{H}_{ee}$ models the electron-electron interaction, $\hat{H}_{eb}$ represents the interaction between electrons and the positive background charge, and the operator $\hat{H}_{bb}$ gives the interaction energy of the background charge with itself.

Similarly as in Refs. [22, 29–31, 35], we approximate the homogeneous electron gas by a finite hypercube filled with electrons. The summation over an infinite number of Coulomb interaction terms can be efficiently calculated using, for example, Ewald's summation technique [10, 19]. In Ewald's approach, the Coulomb interaction is split into a short-ranged part, which is calculated in real space, and a long-ranged part, which is summed in Fourier space. The kinetic energy operator is

$$\hat{H}_{\text{kin}} = -\frac{\hbar^2}{2m} \sum_{i=1}^{N} \nabla_i^2, \tag{2}$$

where the sum is taken over all particles in the finite box. The Ewald electron-electron interaction operator can be

written as [12]

$$\hat{H}_{ee} = \sum_{i<j}^{N} v_E\left(\mathbf{r}_i - \mathbf{r}_j\right) + \frac{1}{2}Nv_0, \tag{3}$$

where $v_E(\mathbf{r})$ is the effective two-body interaction and v_0 is the self-interaction, defined as $v_0 = \lim_{\mathbf{r}\to 0}\{v_E(\mathbf{r}) - 1/r\}$. The negative electron charges are neutralized by a positive, homogeneous background charge. Fraser *et al.* explain [10] how the electron-background and background-background terms, $\hat{H}_{eb}$ and $\hat{H}_{bb}$, vanish when using Ewald's interaction for the three-dimensional electron gas. Using the same arguments, one can show that these terms are also zero in the corresponding two-dimensional system.

In the three-dimensional electron gas, the Ewald interaction is [12]

$$\begin{aligned} v_E(\mathbf{r}) = &\sum_{\mathbf{k}\neq\mathbf{0}} \frac{4\pi}{L^3k^2} e^{i\mathbf{k}\cdot\mathbf{r}} e^{-\eta^2k^2/4} \\ &+ \sum_{\mathbf{R}} \frac{1}{|\mathbf{r}-\mathbf{R}|}\operatorname{erfc}\left(\frac{|\mathbf{r}-\mathbf{R}|}{\eta}\right) - \frac{\pi\eta^2}{L^3}, \end{aligned} \tag{4}$$

where L is the box side length, $\operatorname{erfc}(x)$ is the complementary error function, and η is a free parameter that can take any value in the interval $(0,\infty)$. The translational vector

$$\mathbf{R} = L\left(n_x\mathbf{u}_x + n_y\mathbf{u}_y + n_z\mathbf{u}_z\right), \tag{5}$$

where $\mathbf{u}_i$ is the unit vector for dimension i, is defined for all integers n_x, n_y, and n_z. These vectors are used to obtain all image cells in the entire real space. The parameter η decides how the Coulomb interaction is divided into a short-ranged and long-ranged part, and does not alter the total function. However, the number of operations needed to calculate the Ewald interaction with a desired accuracy depends on η, and η is therefore often chosen to optimize the convergency as a function of the simulation-cell size [12]. In our calculations, we choose η to be an infinitesimally small positive number, similarly as was done in Refs. [22, 29–31, 35]. This gives an interaction that is evaluated only in Fourier space.

When studying the two-dimensional electron gas, we use an Ewald interaction that is quasi two-dimensional. The interaction is derived in three dimensions, with Fourier discretization in only two dimensions [20]. The Ewald effective interaction has the form [20]

$$\begin{aligned} v_E(\mathbf{r}) = &\sum_{\mathbf{k}\neq\mathbf{0}} \frac{\pi}{L^2k}\left\{e^{-kz}\operatorname{erfc}\left(\frac{\eta k}{2} - \frac{z}{\eta}\right) + \right. \\ &\left. e^{kz}\operatorname{erfc}\left(\frac{\eta k}{2} + \frac{z}{\eta}\right)\right\} e^{i\mathbf{k}\cdot\mathbf{r}_{xy}} \\ &+ \sum_{\mathbf{R}} \frac{1}{|\mathbf{r}-\mathbf{R}|}\operatorname{erfc}\left(\frac{|\mathbf{r}-\mathbf{R}|}{\eta}\right) \\ &- \frac{2\pi}{L^2}\left\{z\operatorname{erf}\left(\frac{z}{\eta}\right) + \frac{\eta}{\sqrt{\pi}}e^{-z^2/\eta^2}\right\}, \end{aligned} \tag{6}$$

where the Fourier vectors $\mathbf{k}$ and the position vector $\mathbf{r}_{xy}$ are defined in the (x,y) plane. When applying the interaction $v_E(\mathbf{r})$ to two-dimensional systems, we set z to zero. Similarly as in the three-dimensional case, and as suggested in Ref. [12] for two dimensions, also here we choose η to approach zero from above. The resulting Fourier-transformed interaction is

$$v_E^{\eta=0,z=0}(\mathbf{r}) = \sum_{\mathbf{k}\neq\mathbf{0}} \frac{2\pi}{L^2k} e^{i\mathbf{k}\cdot\mathbf{r}_{xy}}. \tag{7}$$

The self-interaction v_0 is a constant that can be included in the reference energy.

In the three-dimensional electron gas, the antisymmetrized matrix elements are

$$\begin{aligned} &\langle \mathbf{k}_p m_{s_p} \mathbf{k}_q m_{s_q} | \tilde{v} | \mathbf{k}_r m_{s_r} \mathbf{k}_s m_{s_s} \rangle_{AS} \\ &= \frac{4\pi}{L^3}\delta_{\mathbf{k}_p+\mathbf{k}_q,\mathbf{k}_r+\mathbf{k}_s}\left\{\delta_{m_{s_p}m_{s_r}}\delta_{m_{s_q}m_{s_s}}\left(1-\delta_{\mathbf{k}_p\mathbf{k}_r}\right)\frac{1}{|\mathbf{k}_r-\mathbf{k}_p|^2}\right. \\ &\left. -\delta_{m_{s_p}m_{s_s}}\delta_{m_{s_q}m_{s_r}}\left(1-\delta_{\mathbf{k}_p\mathbf{k}_s}\right)\frac{1}{|\mathbf{k}_s-\mathbf{k}_p|^2}\right\}, \end{aligned} \tag{8}$$

where the Kronecker delta functions $\delta_{\mathbf{k}_p\mathbf{k}_r}$ and $\delta_{\mathbf{k}_p\mathbf{k}_s}$ ensure that the contribution with zero momentum transfer vanishes. Similarly, the matrix elements for the two-dimensional electron gas are

$$\begin{aligned} &\langle \mathbf{k}_p m_{s_p} \mathbf{k}_q m_{s_q} | v | \mathbf{k}_r m_{s_r} \mathbf{k}_s m_{s_s} \rangle_{AS} \\ &= \frac{2\pi}{L^2}\delta_{\mathbf{k}_p+\mathbf{k}_q,\mathbf{k}_r+\mathbf{k}_s}\left\{\delta_{m_{s_p}m_{s_r}}\delta_{m_{s_q}m_{s_s}}\left(1-\delta_{\mathbf{k}_p\mathbf{k}_r}\right)\frac{1}{|\mathbf{k}_r-\mathbf{k}_p|}\right. \\ &\left. -\delta_{m_{s_p}m_{s_s}}\delta_{m_{s_q}m_{s_r}}\left(1-\delta_{\mathbf{k}_p\mathbf{k}_s}\right)\frac{1}{|\mathbf{k}_s-\mathbf{k}_p|}\right\}, \end{aligned} \tag{9}$$

where the single-particle momentum vectors $\mathbf{k}_{p,q,r,s}$ are now defined in two dimensions. In our calculations, the self-interaction constant is included in the reference energy, as in Eq. (**??**). We therefore get the Fock-operator matrix elements

$$\langle \mathbf{k}_p | f | \mathbf{k}_q \rangle = \frac{\hbar^2 k_p^2}{2m}\delta_{\mathbf{k}_p,\mathbf{k}_q} + \sum_{\mathbf{k}_i}\langle \mathbf{k}_p\mathbf{k}_i | v | \mathbf{k}_q\mathbf{k}_i\rangle_{AS}. \tag{10}$$

In Ref. [30], the matrix elements were defined with the self-interaction constant included in the two-body interaction. This gives Fock-operator matrix elements with a gap constant. The definition used in Ref. [30] may give numerically more stable calculations, as the gap constant prevents the energy denominator from becoming too small in the vicinity of the Fermi surface. However, when using Fock matrix elements as defined in Eq. (10), the energy denominator in the CC equations never vanishes unless the numerator is zero. When using periodic boundary conditions, the discrete-momentum single-particle basis functions

$$\phi_{\mathbf{k}}(\mathbf{r}) = e^{i\mathbf{k}\cdot\mathbf{r}}/L^{d/2}$$

$n_x^2+n_y^2$	n_x	n_y	$N_{\uparrow\downarrow}$	$N_{\uparrow\uparrow}$
0	0	0	2	1
1	-1	0		
	1	0		
	0	-1		
	0	1	10	5
2	-1	-1		
	-1	1		
	1	-1		
	1	1	18	9
4	-2	0		
	2	0		
	0	-2		
	0	2	26	13
5	-2	-1		
	2	-1		
	-2	1		
	2	1		
	-1	-2		
	-1	2		
	1	-2		
	1	2	42	21

TABLE I. Illustration of how single-particle energies fill energy shells in a two-dimensional electron box. Here n_x and n_y are the momentum quantum numbers, $n_x^2+n_y^2$ determines the single-particle energy level, $N_{\uparrow\downarrow}$ represents the cumulated number of spin-orbitals in an unpolarized spin phase, and $N_{\uparrow\uparrow}$ stands for the cumulated number of spin-orbitals in a spin-polarized system.

are associated with the single-particle energy

$$\varepsilon_{n_x,n_y} = \frac{\hbar^2}{2m}\left(\frac{2\pi}{L}\right)^2\left(n_x^2+n_y^2\right) \tag{11}$$

for two-dimensional sytems and

$$\varepsilon_{n_x,n_y,n_z} = \frac{\hbar^2}{2m}\left(\frac{2\pi}{L}\right)^2\left(n_x^2+n_y^2+n_z^2\right) \tag{12}$$

for three-dimensional systems. Similarly as in, for example, Refs. [2, 13, 35], we choose the single-particle basis such that both the occupied and unoccupied single-particle spaces have a closed-shell structure. This means that all single-particle states corresponding to energies below a chosen cutoff are included in the basis. We study only the unpolarized spin phase, in which all orbitals are occupied with one spin-up and one spin-down electron. Table I shows the lowest-lying spin-orbitals and the cumulated numbers of single-particle states for a two-dimensional electron box with periodic boundary conditions.

Finally, a useful benchmark for our calculations is the expression for the reference energy E_0 per particle. Defining the $T=0$ density ρ_0, we can in turn determine in three dimensions the radius r_0 of a sphere representing the volume an electron occupies (the classical electron radius) as

$$r_0 = \left(\frac{3}{4\pi\rho}\right)^{1/3}.$$

In two dimensions the corresponding quantity is

$$r_0 = \left(\frac{1}{\pi\rho}\right)^{1/2}.$$

One can then express the reference energy per electron in terms of the dimensionless quantity $r_s = r_0/a_0$, where we have introduced the Bohr radius $a_0 = \hbar^2/e^2m$. The energy per electron computed with the reference Slater determinant can then be written as [36] (using hereafter only atomic units, meaning that $\hbar = m = e = 1$)

$$E_0/N = \frac{1}{2}\left[\frac{2.21}{r_s^2} - \frac{0.916}{r_s}\right],$$

for the three-dimensional electron gas. For the two-dimensional gas the corresponding expression is, see for example Refs. [5, 32],

$$E_0/N = \frac{1}{r_s^2} - \frac{8\sqrt{2}}{3\pi r_s}.$$

For an infinite homogeneous system, there are some particular simplications due to the conservation of the total momentum of the particles. By symmetry considerations, the total momentum of the system has to be zero zero. Both the kinetic energy operator and the total Hamiltonian $\hat{H}$ are assumed to be diagonal in the total momentum $\mathbf{K}$. Hence, both the reference state Φ_0 and the correlated ground state Ψ must be eigenfunctions of the operator $\hat{\mathbf{K}}$ with the corresponding eigenvalue $\mathbf{K} = \mathbf{0}$ [37]. This leads to important simplications to our different many-body methods. In coupled cluster theory for example, see the discussion in the next subsection, all terms that involve single particle-hole excitations vanish.

C. Coupled-cluster theory for the homogeneous electron gas

In this subsection we present the coupled-cluster equations needed to obtain the correlation energy at the singles and doubles level. Due to conservation of momentum, the coupled cluster equations simplify considerably. The so-called singles equa

The foundation for most many-body methods is to express the correct wave function by an expansion in a set of basis functions. One example is the Hartree-Fock (HF) method which employs a unitary transformation of the single-particle wave functions,

$$|\lambda\rangle = \sum_{\psi} C_{\lambda\psi}|\psi\rangle, \tag{13}$$

and approximates the ground state with a reference Slater determinant built up by these transformed wave functions. Another example is configuration interaction (CI) where the reference determinant is set to a linear expansion of determinants, including the initial reference determinant, 1p-1h excitations, 2p-2h excitations and so on, i.e.

$$|\Psi_0^{CI}\rangle = C_0|\Phi_0\rangle + \sum_{ia} C_i^a|\Phi_i^a\rangle + \sum_{ijab} C_{ij}^{ab}|\Phi_{ij}^{ab}\rangle + \cdots \quad . \tag{14}$$

In all these methods one needs to solve a set of coupled equations to find the coefficients.

The coupled-cluster method also expands the exact solution in a set of Slater determinants, but employs a nonlinear expansion through the exponential ansatz,

$$|\Psi_0^{CC}\rangle = e^{\hat{T}}|\Phi_0\rangle, \tag{15}$$

where $\hat{T}$ is the cluster operator including *all* possible excitations on the reference determinant. Sorting excitations by the number of excited electrons, we may generally express this general cluster operator as a sum of a 1p-1h operator, a 2p-2h operator, and so on,

$$\hat{T} = \hat{T}_1 + \hat{T}_2 + \hat{T}_3 + \cdots \quad . \tag{16}$$

In the form of second-quantized operators the 1p-1h cluster operator is defined as

$$\hat{T}_1 = \sum_{ia} t_i^a \hat{a}^\dagger \hat{i}, \tag{17}$$

the 2p-2h cluster operator as

$$\hat{T}_2 = \frac{1}{4}\sum_{ijab} t_{ij}^{ab} \hat{a}^\dagger \hat{b}^\dagger \hat{j}\hat{i}, \tag{18}$$

continuing up to

$$\hat{T}_n = \left(\frac{1}{n!}\right)^2 \sum_{ij\cdots ab\cdots} t_{ij\cdots}^{ab\cdots} \hat{a}^\dagger \hat{b}^\dagger \cdots \hat{j}\hat{i}. \tag{19}$$

As long as we have a complete single-particle basis and include all possible excitations up to np-nh in a system with n particles, we should find the exact solution for both CI, $|\Psi_0^{CI}\rangle$, and CC, $|\Psi_0^{CC}\rangle$.

Adding all terms together we get the complete $\hat{T}_1$ amplitude equations;

$$\begin{aligned}
0 =& f_{ai} + \sum_d f_{ad} t_i^d - \sum_l f_{li} t_l^a + \sum_{ld} \langle la||di\rangle t_l^d \\
&+ \sum_{ld} f_{ld} t_{il}^{ad} + \frac{1}{2}\sum_{lde} \langle al||de\rangle t_{il}^{de} - \frac{1}{2}\sum_{lmd} \langle lm||di\rangle t_{lm}^{da} - \sum_{ld} f_{ld} t_i^d t_l^a \\
&+ \sum_{lde} \langle al||de\rangle t_i^d t_l^e - \sum_{lmd} \langle lm||di\rangle t_l^d t_m^a + \frac{1}{2}\sum_{lmde} \langle lm||de\rangle t_i^d t_{lm}^{ea} \\
&+ \frac{1}{2}\sum_{lmde} \langle lm||de\rangle t_m^a t_{il}^{de} + \sum_{lmde} \langle lm||de\rangle t_m^e t_{il}^{ad} + \sum_{lmde} \langle lm||de\rangle t_i^d t_l^e t_m^a.
\end{aligned} \tag{20}$$

$$\begin{aligned}
0 =& \langle ab||ij\rangle + \frac{1}{2}\langle ab||de\rangle t_{ij}^{de} \\
&- \hat{P}_{ij}\left[f_{li} + f_{ld} t_i^d + \langle ml||di\rangle t_m^d + \langle ml||de\rangle t_m^d t_i^e + \frac{1}{2}\langle ml||de\rangle t_{mi}^{de}\right] t_{l} \\
&+ \frac{1}{2}\left[\langle lm||ij\rangle + \hat{P}_{ij}\langle lm||dj\rangle t_i^d + \frac{1}{2}\langle lm||de\rangle t_{ij}^{de} + \hat{P}_{ij}\frac{1}{2}\langle lm||de\rangle t_i^d t_j^e\right. \\
&+ \hat{P}_{ab}\left[f_{bd} - f_{ld} t_l^b + \langle bl||de\rangle t_l^e - \langle lm||de\rangle t_m^e t_l^b + \frac{1}{2}\langle lm||de\rangle t_{lm}^{eb}\right] t_{ij}^{a} \\
&+ \hat{P}_{ij}\hat{P}_{ab}\left[\langle lb||dj\rangle - \langle lm||dj\rangle t_m^b + \langle bl||ed\rangle t_j^e - \langle lm||de\rangle t_j^e t_m^b + \frac{1}{2}\langle lm \right. \\
&- \hat{P}_{ab}\left[\langle al||ij\rangle + \frac{1}{2}\langle al||de\rangle t_{ij}^{de} + \hat{P}_{ij}\langle al||dj\rangle t_i^d + \hat{P}_{ij}\frac{1}{2}\langle al||de\rangle t_i^d t_j^e \right. \\
&+ \frac{1}{2}\langle lm||ij\rangle t_m^a + \frac{1}{4}\langle lm||de\rangle t_m^a t_{ij}^{de} + \hat{P}_{ij}\frac{1}{2}\langle lm||dj\rangle t_i^d t_m^a + \hat{P}_{ij}\frac{1}{4}\langle lm|| \\
&+ \hat{P}_{ij}\left[\langle ab||dj\rangle + \frac{1}{2}\langle ab||de\rangle t_j^e\right] t_i^d.
\end{aligned} \tag{21}$$

D. The Similarity Renormalization Group flow equations

The Similarity Renormalization Group (SRG) method was introduced independently by Glazek and Wilson [38] and Wegner [39] as a new way to implement the principle of energy scale separation. The method uses a continuous sequence of unitary transformations to decouple the high- and low-energy matrix elements of a given interaction, thus driving the Hamiltonian towards a band- or block-diagonal form.

Let us consider the initial Hamiltonian

$$\hat{H} = \hat{H}^{\mathrm{d}} + \hat{H}^{\mathrm{od}},$$

where $\hat{H}^{\mathrm{d}}$ and $\hat{H}^{\mathrm{od}}$ denote its "diagonal" and "off-diagonal" parts, respectively. Introducing a flow parameter s, there exits a unitary transformation U_s, such that

$$\hat{H}_s = U_s^\dagger \hat{H} U_s \equiv \hat{H}_s^{\mathrm{d}} + \hat{H}_s^{\mathrm{od}}, \tag{22}$$

with the relations $U_{s=0} = \mathbf{1}$, and $\hat{H}_{s=0} = \hat{H}$. The transformation U_s is parametrized as

$$U_s = T_s \exp\left(\int_0^s ds' \hat{\eta}_{s'}\right),$$

where the anti-hermitian operator $\hat{\eta}_s$ serves as generator of the transformation. With T_s we denote s-ordering, which is defined equivalently to usual time-ordering. Taking the derivative of $\hat{H}_s$ with respect to s gives

$$\frac{d\hat{H}_s}{ds} = \frac{dU_s}{ds}\hat{H}U_s^\dagger + U_s\hat{H}\frac{dU_s^\dagger}{ds}. \tag{23}$$

Utilizing that for our particular form of U_s, we have that

$$\hat{\eta}_s = \frac{dU_s}{ds}U_s^\dagger = -U_s\frac{dU_s^\dagger}{ds} = -\hat{\eta}_s, \tag{24}$$

we obtain that

$$\frac{d\hat{H}_s}{ds} = \hat{\eta}_s\hat{H}_s - \hat{H}_s\hat{\eta}_s = \left[\hat{\eta}_s, \hat{H}_s\right]. \tag{25}$$

This is the key expression of the SRG method, describing the flow of the Hamiltonian. The specific unitary transformation is determined by the choice of $\hat{\eta}_s$. Through different choices of $\hat{\eta}_s$, the SRG evolution can be adapted to the features of a particular problem.

One possibility to solve the flow equations is to choose a basis with respect to the physical vacuum state, set up the Hamiltonian matrix in this basis and solve Eq. (25) as a set of coupled first-order differential equations. However, since the size of the problem grows enormously with the number of particles and the size of the model space, the applicability of this free-space SRG method is restricted to comparatively small systems.

Instead of performing SRG in free space, the evolution can be done at finite density, i.e. directly in the N-body system [40]. This approach has recently been applied very successfully in nuclear physics [41, 42] and is called in-medium SRG (IM-SRG). The method allows the evolution of $3, ..., N$-body operators using only two-body machinery, with the simplifications arising from the use of normal-ordering with respect to a reference state.

Integrating the flow equations (25), we face one of the major challenges of the SRG method, namely the generation of higher and higher order interaction terms during the flow. With each evaluation of the commutator, the Hamiltonian gains terms of higher order, and these induced contributions will in subsequent integration steps contribute to terms of lower order. In principle, this continues to infinity.
To make the method computationally possible, we have to close the IM-SRG flow equations, suggesting that we are forced to truncate the equations to a certain order. We choose to truncate both $\hat{H}_s$ and $\hat{\eta}_s$ at the two-body level, an approach which is referred to as IM-SRG(2). This normal-ordered two-body approximation seems to be sufficient in many cases and has yielded excellent results for several nuclei [41**?** , 42].
The commutator in the flow equations (25) guarantees that the IM-SRG wave function $U_s^\dagger|\Phi\rangle$ can be expanded in terms of linked diagrams only [28**?**], which suggests that IM-SRG is size-extensive. Regarding the quality of the SRG results, it means that the error introduced by truncating the many-body expansions scales linearly with the number of particles N. With this truncation, the generator $\hat{\eta}$ can be written as where $\eta^{(1)}_{pq}$ and $\eta^{(2)}_{pqrs}$ are the one- and two-body elements, respectively. Making use of the permutation operator $\hat{P}_{pq}f(p,q) = f(q,p)$, the IM-SRG(2) flow equations are given by Note that for brevity, we skipped all s-dependence in the equations.

Choice of generator

To determine the specific unitary transformation, one needs to specify the generator $\hat{\eta}$. Through different choices, the SRG flow can be adapted to the features of a particular problem.

Apart from this canonical generator, there exist several other ones in literature. One of them is White's choice [43], which makes numerical approaches much more efficient. The problem with Wegner's generator are the widely varying decaying speeds of the elements, removing first terms with large energy differences and then subsequently those ones with smaller energy separations. That way the flow equations become a stiff set of coupled differential equations, which often gets numerically unstable. White takes an alternative approach, which is especially suited for problems where one is interested in the ground state of a system. Instead of driving all off-diagonal elements of the Hamiltonian to zero, he focuses solely on those ones that are connected to the reference state $|\Phi_0\rangle$, aiming to decouple the reference state from the remaining Hamiltonian. With a suitable transformation, the elements get similar decaying speeds, which solves the problem of stiffness of the flow equations. The generator is explicitly constructed the following way [42, 43]

$$\begin{aligned}\hat{\eta} = &\sum_{ai} \frac{f_{ai}}{f_a - f_i - v_{aiai}}\{a_a\dagger a_i\} - \text{hc} \\ &+ \sum_{abij} \frac{v_{abij}}{f_a + f_b - f_i - f_j + A_{abij}}\{a_a\dagger a_b\dagger a_j a_i\} - \text{hc},\end{aligned} \tag{26}$$

with $f_p \equiv f_{pp}$, 'hc' denoting the Hermitian conjugate, and

$$A_{abij} = v_{abab} + v_{ijij} - v_{aiai} - v_{ajaj} - v_{bibi} - v_{bjbj}.$$

Compared to Wegner's canonical generator, where the final flow equations involve third order powers of the f- and v-elements, these elements contribute only linearly with White's generator, which results in much better numerical properties.

E. The FCIQMC algorithm

The recently developed Full Configuration Interaction Quantum Monte Carlo (FCIQMC) [1, 2, 44] promises to calculate the Full Configuration Interaction (FCI) ground state energy within a given Hilbert space, and often at a much lower computational cost than conventional FCI solvers. The FCI energy is given by the equation

$$E_0^{FCI} = \min\langle\Psi|\hat{H}|\Psi\rangle, \tag{27}$$

with $|\Psi\rangle \in \mathcal{H}_{FCI}$. The FCI space $\mathcal{H}_{FCI}$ is spanned by all determinants that can be constructed from single-particle

states with an energy lower than the cutoff $\mathbf{k}_c^2/2$. This problem is usually solved by using brute force diagonalizion techniques like the Lanczos algorithm [mat. comp.], but due to the large memory footprint of such methods, these are limited to systems with "small" Hilbert spaces. The largest simulations of this kind is performed with a basis with up to $\sim 10^{11}$(?) determinants [? ?] which in practice means that only systems with a relatively low number of particles or small single particle basis can be simulated. The FCIQMC algorithm does however make it possible threat much larger Hilbert spaces. One example is the simulations performed by Shepherd *et. al.* [23] where the algorithm is applied on the three dimensional homogenous electron gas with a bases consisting of up to $\sim 10^{108}$ determinants.

In the following we will briefly introduce the FCIQMC algorithm. This is a so called Projector Monte Carlo algorithm where the FCI ground state is found by calculating the projected state

$$\lim_{t\to\infty} e^{-t(\hat{H}-S)}|\Psi_0\rangle, \tag{28}$$

where the shift $S \in \mathcal{R}$. The projected state will be proportional to the FCI ground state Ψ_0^{FCI} if the shift is equal to E_0^{FCI} and $\langle\Psi_0|\Psi_0^{FCI}\rangle \neq 0$. This is the same approach that is used in other Projector Monte Carlo methods like Diffusion Monte Carlo or Greens Function Monte Carlo, but the integration is not performed in the coordinate space but in the discrete space of Slater determinants. Because of the inherent anti-symmetric properties of this basis, the infamous sign problem is not as severe for FCIQMC as for other Projector Monte Carlo methods, and in principle the exact FCI energies can be calculated. See for example Refs. [45, 46] for a thorough analysis of the sign problem in FCIQMC.

The large t projected state is found by iterating over the equation

$$|\Psi_0\rangle \leftarrow e^{-\tau(\hat{H}-S)}|\Psi_0\rangle, \tag{29}$$

where τ is a small time step. The initial state $|\Psi_0\rangle$ is now expanded on the FCI basis

$$|\Psi_0\rangle = \sum_i C_i|\Phi_i\rangle, \tag{30}$$

and by approximating the projection operator as its first order Taylor expansion we can write Eq. (29) in terms of the coefficients $\{C_i\}$

$$C_i \leftarrow C_i - \sum_j p_d(i|j)C_j, \tag{31}$$

where we have used $p_d(i|j) = \tau(\hat{H}_{ij} - S\delta_{ij})$ and $H_{ij} = \langle\Phi_i|\hat{H}|\Phi_j\rangle$. In the limit of a large number of iterations, the coefficients $\{C_i\}$ will be proportional to those of the ground state. Note that this approach is exact when the time step τ is smaller than $2/(E_M - S)$, where E_M is the largest single particle energy $E_M = \max(\langle\Phi_i|\hat{H}|\Phi_i\rangle)$.

A DMC inspired approach is used to find the steady state solution of Eq. (31). The coefficients $\{C_i\}$ are represented by a population of N_W walkers α which are distributed on the determinants Φ_{i_α} and with a sign $s_\alpha = \pm$. The amplitude $\{C_i\}$ is then defined to be

$$C_i \propto n_i = \sum_\alpha s_\alpha \delta_{ii_\alpha}, \tag{32}$$

which is a signed sum where two walkers of opposite signs on the same determinant will make zero contribution.

It is now possible to define a set of dynamical rules for the walkers of such a nature that they converge to a distribution $(n_1, n_2, \dots) \propto (C_1, C_2, \dots)$. These dynamical rules are derived from the last term of the right hand side of Eq. (31) which describes the rate of which the coefficients C_i changes during one iteration.

Numerically we do the following. Given a walker on determinant j, we add $N_a = \text{floor}(|p_d(i|j)|)$ walkers on determinant i, and one extra with the probability $N_a - |p_d(i|j)|$. The new walkers have the same sign as the walker on determinant j is $p_d(i|j)$ is negative and the opposite sign otherwise.

The sum over all elements $p_d(i|j)$ is numerically very expensive for large FCI bases, and to be able to solve Eq. (31) efficiently, Monte Carlo sampling is used to approximate the sum over the off diagonal terms

$$\sum_j \sum_{i\neq j} p_d(i|j)C_j \approx \sum_j \sum_{s\in\mathcal{S}_j} p_d(s|j)/p_{gen}(s|j)C_j, \tag{33}$$

where $p_{gen}(s|j)$ is the suggestion probability of s from j, and $\mathcal{S}_j$ consists of n_j elements that are sampled from $p_{gen}(s|j)$. This reduce the number of operations to $\mathcal{O}(N_w)$ each iteration. This equation is only correct when $p_{gen}(s|j)$ is different from zero for all connected determinants $|\Phi_j\rangle$ and $|\Phi_s\rangle$

$$p_{gen}(s|j) \neq 0 \quad \forall \quad H_{js} \neq 0. \tag{34}$$

In principle, there is no other constraint on $p_{gen}(s|j)$, and as long as the number of iterations is large enough the simulations will eventually converge to the correct results, but in practice certain choices of suggestion probability distributions are expected to lead to a more efficient sampling. In our implementation we have used a $p_{gen}(s|j)$ which is uniform for all s that corresponds to an interaction $\langle\Phi_s|\hat{H}|\Phi_j\rangle$ where the spin and momentum are conserved and zero otherwise.

1. *The initiator-FCIQMC algorithm*

It has been shown that the number of walkers must be above a certain threshold N_C for the population to converge to the ground state distribution [46**?**]. This number is known to be highly system dependent and to

increase roughly linearly with the size of the FCI space [**?**].

Cleland *et. al.* (2010) [44] demonstrated that by introducing a set of new dynamical rules for the walkers, the performance of the algorithm can be improved drastically while still obtaining results with a precision of 10^{-3} Ry or better. The number of walkers that is necessary in such simulations are typically several orders of magnitude smaller than N_C. The improved algorithm is called initiator-FCIQMC or i-FCIQMC, and does only differ from the original algorithm in how the spawning probabilites $\{p_d(i|j); i \neq j\}$ are calculated.

First, a so called initiator space is defined. This is a set of determinants which are assumed to have a relatively large average population (large ampiludes $|C_i|$). All walkers that live on a determinant in the initiator space are called initiators, and initiators follows the same rules as walkers in the basic FCIQMC algorithm. The first rule of i-FCIQMC concerns the non-initiators and states that:

- (*Spawning rule I*): Non-initiators are only allowed to spawn on determinants that are previously populated.

With this rule the Hilbert space is in effect reduced to the states in the initiator space and the single and double excitations of these. Next, two additional rules are added to improve the energy and to give the walkers access to the entire FCI space:

- (*Dynamic enlargement of the initiator space*): We introduce the initiator threshold N_I which is a parameter that is set before a simulations is started. All determinants Φ_i with a population $|n_i| \geq N_I$ are automatically included in the initiator space for as long the population is above this limit. Here n_i is the signed population of Φ_i. positive integer that we will refer to as the initiator threshold. The initiator threshold is set before the simulation is started. identical to FCIQMC.

- (*Spawning rule II*): If the absolute value of the signed sum $\sum_\alpha s_\alpha$ of non-initiator walkers α that attempts to spawn on an unpopulated determinant is larger than two, then these spawning events are accepted.

Although the initiator adaption of the algorithm has been shown to increase the efficiency, it is only correct according to Eq. (31) in the limit of a large number of of walkers or an initiator threshold $N_I = 1$. In this case the initiator space will grow to include the entire FCI space, and i-FCIQMC will tend to FCIQMC. This means that the i-FCIQMC energies are systematically improvable and that the so called initiator error will decay to zero when the number of walkers is increased.

The initiator spaces are defined using a so called Complete Active Space (CAS) criterion, which is often used within quantum chemistry together with methods like many-body pertubation theory or the configuration interaction method to pick out physically relevant states of a Hilbert space. Because of the dynamic enlargement of the initiator space, the final result will be the same regardles of which CAS we choose. But, as Cleland *et. al.* [44] has shown, an appropriate CAS might sometimes improve the convergence.

2. Population control and the statistical estimators

The population of walkers will on average increase if the shift S is larger than E_0^{FCI} and decrease if S is smaller than E_0^{FCI}. We can therefore control the population by varying S. We use the formula of Umrigar *et al* [47] which has been used for population control in the context of DMC

$$S \to S^{(i)} = S^{(i-1)} - \frac{\xi}{\tau} \log \left[\frac{N_W^{(i)}}{N_W^{(i-1)}} \right], \tag{35}$$

where ξ is a real number of which the optimal value must be found by experiment, and $N_W^{(i)}$ and $S^{(i)}$ are the population and shift at the time $i\tau$. The shift S that stabilizes the number of walkers must be the ground state energy, and this means that the above equation provides us with a measure of E_0^{FCI}.

We use two different statistical estimators to calculate the energy. The first is the one that we just mentioned, which can be taken as the long time average of the shift

$$E_0 \approx \langle S \rangle = (1/N) \sum_{i=1}^{N} S^{(i)}, \tag{36}$$

and which we will refer to as the generational estimator of the energy. The second is the projected estimator that is calculated by sampling the projected energy

$$E_0 = \frac{\langle \Phi_0 | \hat{H} | \Psi_0^{FCI} \rangle}{\langle \Phi_0 | \Psi_0^{FCI} \rangle} = \frac{\langle \Phi_0 | \hat{H} \sum_i C_i | \Phi_i \rangle}{\langle \Phi_0 | \sum_i C_i | \Phi_i \rangle}, \tag{37}$$

which is rewritten on the form

$$E_0 \approx \langle E_P \rangle = H_{00} + \sum_{i \neq 0} H_{0i} \langle n_i \rangle / \langle n_0 \rangle. \tag{38}$$

3. Simulation procedures

A FCIQMC or i-FCIQMC simulation is usually started with one walker on the Hartree-Fock (HF) determinant and a shift S that is equal to the HF energy. Since the HF energy is larger than the FCI energy, the number of walkers N_W will increase rapidly. To stop the population growth and stabilize the population around the desired number of walkers, the shift S is adjusted according to Eq. (36). After a thermalization phase we start sampling the generational and the projected estimator.

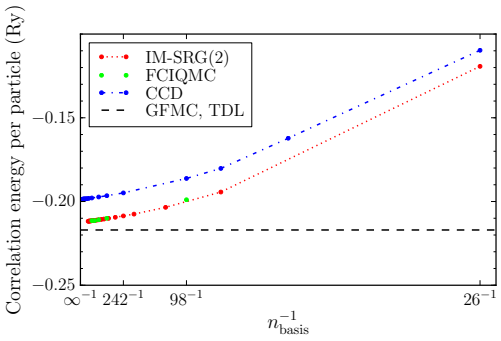

FIG. 1. Correlation energy per particle as function of the number of single-particle orbits for a ten-particle electron gas at $r_s = 1.0$, using CCD, IMSRG(2) and FCIQMC. The IMSRG(2) correlation energies are in excellent agreement with the almost exact FCIQMC results. For comparison, we have marked the correlation energy in the thermodynamic limit, as obtained by extrapolating GFMC energies. The width of the horizontal line shows the statistical error of the GFMC calculations.

These estimators are statistical measures, and there will always be a certain statistical error associated with them. The statistical errors of both estimators are calculated using Flyvbjerg-Pedersen analysis [citation], and the energy with the smallest statistical error is chosen as the final result.

A series of simulations with an increasing number of walkers must be performed to converge the i-FCIQMC energy. (A study of the convergence of the initiator error is provided by Sheperd *et. al.* [23]).

III. RESULTS

A. Benchmark results for the three-dimensional electron gas

B. The two-dimensional electron gas

IV. CONCLUSIONS

ACKNOWLEDGMENTS

This work was supported by the Research Council of Norway under contract ISP-Fysikk/216699. This research used computational resources of the Notur project in Norway.

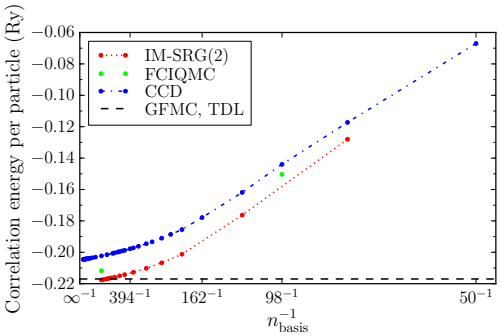

FIG. 2. Correlation energy per particle as function of the number of single-particle orbits for a 26 particle electron gas at $r_s = 1.0$, using CCD, IMSRG(2) and FCIQMC. Here we see a larger discrepancy between the IMSRG(2) results and the FCIQMC values. For comparison, we have marked the correlation energy in the thermodynamic limit, as obtained by extrapolating GFMC energies.

[1] G. H. Booth, A. J. W. Thom, and A. Alavi, J. Chem. Phys. **131**, 054106 (2009)
[2] J. J. Shepherd, G. H. Booth, A. Grüneis, and A. Alavi, Phys. Rev. B **85**, 081103 (2012)
[3] G. H. Booth, A. Grüneis, G. Kresse, and A. Alavi, Nature **493**, 365 (2013)
[4] D. M. Ceperley and B. J. Alder, Phys. Rev. Lett. **45**, 566 (1980)
[5] B. Tanatar and D. M. Ceperley, Phys. Rev. B **39**, 5005 (1989)
[6] E. Wigner, Phys. Rev. **46**, 1002 (1934)
[7] D. Ceperley, Phys. Rev. B **18**, 3126 (1978)
[8] R. F. Bishop and K. H. L"uhrmann, Phys. Rev. B **26**, 5523 (1982)
[9] W. M. C. Foulkes, L. Mitas, R. J. Needs, and G. Rajagopal, Rev. Mod. Phys. **73**, 33 (2001)
[10] L. M. Fraser, W. M. C. Foulkes, G. Rajagopal, R. J. Needs, S. D. Kenny, and A. J. Williamson, Phys. Rev. B **53**, 1814 (1996)
[11] S. Chiesa, D. M. Ceperley, R. M. Martin, and M. Holzmann, Phys. Rev. Lett. **97**, 076404 (2006)
[12] N. D. Drummond, R. J. Needs, A. Sorouri, and W. M. C. Foulkes, Phys. Rev. B **78**, 125106 (2008)
[13] G. Hagen, T. Papenbrock, A. Ekström, K. A. Wendt, G. Baardsen, S. Gandolfi, M. Hjorth-Jensen, and C. J. Horowitz, Phys. Rev. C **89**, 014319 (2014)
[14] M. Gell-Mann and K. A. Brueckner, Phys. Rev. **106**, 364 (1957)
[15] K. S. Singwi, M. P. Tosi, R. H. Land, and A. Sjölander, Phys. Rev. **176**, 589 (1968)
[16] D. N. Lowy and G. E. Brown, Phys. Rev. B **12**, 2138 (1975)
[17] Y. Kwon, D. M. Ceperley, and R. M. Martin, Phys. Rev. B **58**, 6800 (1998)
[18] C. Lin, F. H. Zong, and D. M. Ceperley, Phys. Rev. E **64**, 016702 (2001)
[19] P. P. Ewald, Ann. Phys. **64**, 253 (1921)
[20] B. Wood, W. M. C. Foulkes, M. D. Towler, and N. D.

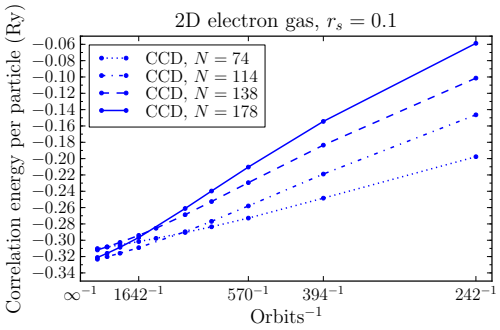

FIG. 3. CCD correlation energy per particle as function of the number of single-particle orbits for varying electron numebrs N $r_s = 0.1$.

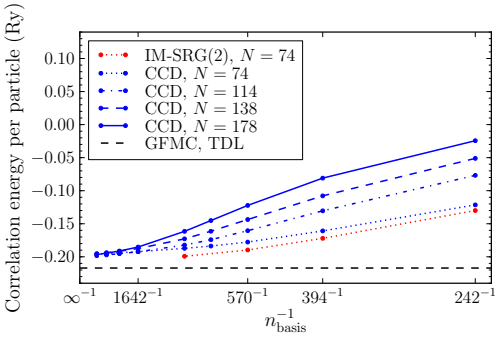

FIG. 5. CCD correlation energy per particle as function of the number of single-particle orbits for varying electron numebrs N $r_s = 1.0$.

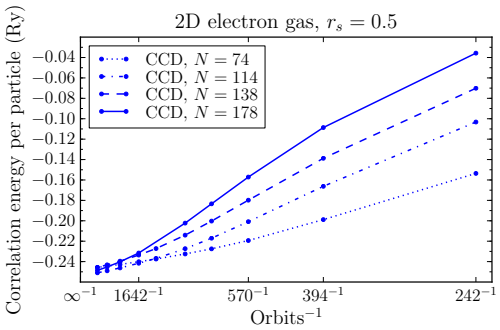

FIG. 4. CCD correlation energy per particle as function of the number of single-particle orbits for varying electron numebrs N $r_s = 0.5$.

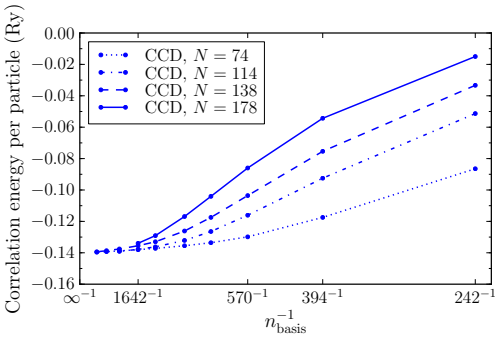

FIG. 6. CCD correlation energy per particle as function of the number of single-particle orbits for varying electron numebrs N $r_s = 2.0$.

Drummond, Journal of Physics: Condensed Matter **16**, 891 (2004)

[21] F. E. Harris, H. J. Monkhorst, and D. L. Freeman, *Algebraic and Diagrammatic Methods in Many-Fermion Theory* (Oxford Press, New York, 1992)

[22] J. J. Shepherd, A. Grüneis, G. H. Booth, G. Kresse, and A. Alavi, Phys. Rev. B **86**, 035111 (2012)

[23] J. J. Shepherd, G. H. Booth, and A. Alavi, J. Chem. Phys. **136**, 244101 (2012)

[24] C. M. Singal and T. P. Das, Phys. Rev. B **8**, 3675 (1973)

[25] M. I. Haftel and F. Tabakin, Nucl. Phys. A **158**, 1 (1970)

[26] D. L. Freeman, Phys. Rev. B **15**, 5512 (1977)

[27] R. F. Bishop and K. H. L"uhrmann, Phys. Rev. B **17**, 3757 (1978)

[28] I. Shavitt and R. J. Bartlett, *Many-body Methods in Chemistry and Physics* (Cambridge University Press, 2009)

[29] J. J. Shepherd and A. Grüneis, Phys. Rev. Lett. **110**, 226401 (2013)

[30] J. J. Shepherd, T. M. Henderson, and G. E. Scuseria, Phys. Rev. Lett. **112**, 209901 (2014)

[31] J. J. Shepherd, T. M. Henderson, and G. E. Scuseria, The Journal of Chemical Physics **140**, 124102 (2014), doi:"bibinfo doi http://dx.doi.org/10.1063/1.4867783

[32] A. K. Rajagopal and J. C. Kimball, Phys. Rev. B **15**, 2819 (1977)

[33] D. L. Freeman, Solid State Commun. **26**, 289 (1978)

[34] D. L. Freeman, J. Phys. C: Solid State Phys. **16**, 711 (1983)

[35] A. Roggero, A. Mukherjee, and F. Pederiva, Phys. Rev. B **88**, 115138 (2013)

[36] A. L. Fetter and J. D. Walecka, *Quantum Theory of Many-Particle Systems* (McGraw-Hill, 1971)

[37] B. D. Day, Rev. Mod. Phys. **39**, 719 (1967)

[38] S. D. Głazek and K. G. Wilson, Phys. Rev. D **48**, 5863 (1993)S. D. Glazek and K. G. Wilson, *ibid.* **49**, 4214 (1994)

[39] F. J. Wegner, Ann. Phys. **3**, 77 (1994)Phys. Rep. **348**, 77 (2001)

[40] S. Kehrein, *The Flow Equation Approach to Many-Particle Systems*, Springer Tracts in Modern Physics (Springer, 2006)

[41] H. Hergert, S. K. Bogner, S. Binder, S. Calci, J. Langhammer, R. Roth, and A. Schwenk, Phys. Rev. C **78**, 014003 (2012)

[42] K. Tsukiyama, S. K. Bogner, and A. Schwenk, Phys. Rev. Lett. **106**, 222502 (2011)

[43] S. R. White, J. Chem. Phys. **117** (2002)

[44] D. Cleland, G. H. Booth, and A. Alavi, J. Chem. Phys. **132**, 041103 (2010)
[45] M. H. Kolodrubetz, J. S. Spencer, B. K. Clark, and W. M. Foulkes, J. Chem. Phys. **138**, 024110 (2013)
[46] J. S. Spencer, N. S. Blunt, and W. M. Foulkes, J. Chem. Phys. **136**, 054110 (2012)
[47] C. J. Umrigar, M. P. Nightingale, and K. J. Runge, J. Chem. Phys. **99**, 2865 (1993)